Cerebral Cortex June 2011;21:1351–1361
doi:10.1093/cercor/bhq214
Advance Access publication November 10, 2010

Development of Inhibitory Timescales in Auditory Cortex

Anne-Marie M. Oswald[1,2] and Alex D. Reyes[1]

[1]Center for Neural Science, New York University, NY 10003, USA and [2]Current address: Department of Biology, Center for the Neural Basis of Cognition, Carnegie Mellon University, Pittsburgh, PA 15213, USA

Address correspondence to Anne-Marie M. Oswald, Department of Biological Sciences and Center for the Neuronal Basis of Cognition, Carnegie Mellon University, 4400 Fifth Avenue, Pittsburgh, PA 15213, USA. Email: ammoswald@gmail.com.

The time course of inhibition plays an important role in cortical sensitivity, tuning, and temporal response properties. We investigated the development of L2/3 inhibitory circuitry between fast-spiking (FS) interneurons and pyramidal cells (PCs) in auditory thalamocortical slices from mice between postnatal day 10 (P10) and P29. We found that the maturation of the intrinsic and synaptic properties of both FS cells and their connected PCs influence the timescales of inhibition. FS cell firing rates increased with age owing to decreased membrane time constants, shorter afterhyperpolarizations, and narrower action potentials. Between FS–PC pairs, excitatory postsynaptic potentials (EPSPs) and inhibitory postsynaptic potentials (IPSPs) changed with age. The latencies, rise, and peak times of the IPSPs, as well as the decay constants of both EPSPs and IPSPs decreased between P10 and P29. In addition, decreases in short-term depression at excitatory PC–FS synapses resulted in more sustained synaptic responses during repetitive stimulation. Finally, we show that during early development, the temporal properties that influence the recruitment of inhibition lag those of excitation. Taken together, our results suggest that the changes in the timescales of inhibitory recruitment coincide with the development of the tuning and temporal response properties of auditory cortical networks.

Keywords: circuitry, fast-spiking interneuron, pyramidal cell, synaptic integration

Introduction

The temporal recruitment of inhibition significantly impacts neural responses during cortical processing. In individual neurons, the precise timing of inhibition with respect to excitation sets the duration of the synaptic integration window (De Ribaupierre et al. 1972; Volkov and Galazjuk 1991; Ojima and Murakami 2002; Wehr and Zador 2003; Higley and Contreras 2006). In auditory cortex (AI), this contributes to frequency and intensity tuning (Wehr and Zador 2003; Tan et al. 2004, 2007; Wu et al. 2006, 2008) and directional tuning to frequency sweeps (Zhang et al. 2003). Furthermore, the duration of inhibitory synaptic inputs can influence responses to repetitive inputs (i.e., masking; Brosch and Schreiner 1997; Wehr and Zador 2005) and oscillatory activity (Traub et al. 1996; Atallah and Scanziani 2009) that arises during acoustic processing (Brosch et al. 2002; Lakatos et al. 2004; Jeschke et al. 2007; Schroeder et al. 2008). Since inhibitory timing is integral to tuning and temporal response properties, we characterized the development of the intrinsic and synaptic properties that underlie the time course of inhibition in AI.

Cortical responses to auditory input change dramatically during development. In rodents, acoustically evoked AI responses at hearing onset (P10–P12, Ehret 1976) are weak and uniformly tuned (de Villers-Sidani et al. 2007). Between P10 and P13, auditory experience markedly impacts cortical development (Chang and Merzenich 2003; Seidl and Grothe 2005; Zhang et al. 2006; de Villers-Sidani et al. 2007), leading to the maturation of the tonotopic map between P14 and P20 (Chang and Merzenich 2003; Zhang et al. 2006; de Villers-Sidani et al. 2007). Excitatory and inhibitory receptive fields, bandwidths, temporal responsiveness, and frequency sweep sensitivities are further refined between P20 and P40 (Chang et al. 2005; Insanally et al. 2009; Dorrn et al. 2010). These changes may, in part, be due to the development of excitatory AI neurons (Metherate and Aramakis 1999; Oswald and Reyes 2008). However, the maturation of inhibition mediated by parvalbumin-positive (PV+) fast-spiking (FS) interneurons may also contribute to the early development of cortical responses (Hensch 2005). FS interneurons are a major source of inhibition in cortical networks due their high probability of connection with pyramidal cells (PCs) (Gonchar et al. 2001; Thomson et al. 2002; Beierlein et al. 2003; Holmgren et al. 2003; Thomson and Lamy 2007; Oswald et al. 2009). In AI, manipulations that impair tonotopic maturation decrease neural synchrony and the proportion of FS cells in the affected frequency band (de Villers-Sidani et al. 2008). Moreover, hearing loss impairs inhibitory development and raises the excitability of AI neurons (Kotak et al. 2005, 2008; Sarro et al. 2008), suggesting that the maturation of inhibition is an essential feature of auditory network responsiveness.

In this study, we examine the development of L2/3 circuitry, which complements previous in vivo studies that focused on the thalamorecipient layers (L3–L5). PCs in the supragranular layers receive direct thalamic inputs in L1 and L3, as well as integrate information from L3 to L5 and other PCs within and across cortical columns and the contralateral hemisphere (Winer 1984, 1985; Code and Winer 1985; Ojima et al. 1991; Metherate and Cruikshank 1999; Linden and Schreiner. 2003; Barbour and Callaway 2008). L2/3 neurons respond to both pure tones and more complex auditory inputs (Volkov and Galazjuk 1991; Ojima and Murakami 2002; Wang et al. 2005). In addition, L2/3 FS–PC circuits have been postulated to support the genesis of oscillatory activity in AI (MacDonald and Barth 1995; Barth and MacDonald 1996; Oswald et al. 2009). Recurrent connectivity within L2/3 provides significant excitatory drive to both PCs and FS cells (Oswald and Reyes 2008; Oswald et al. 2009), and thus, the timing of inhibition could substantially influence the integration of stimulus features as well as network activity. We investigated the development of 3 factors that influence the recruitment of inhibition: the intrinsic properties that govern the FS cell excitability, the excitatory synaptic potentials from PCs to FS cells, and inhibitory synaptic potentials in PCs. We recorded FS cells and PCs in juvenile mice and found that both intrinsic and

synaptic properties changed dramatically between P10 and P29. Moreover, the development of the timescales of inhibitory synapses lagged those of excitatory connections. Our results suggest that the maturation of inhibitory timing contributes to narrowing of synaptic integration windows and increases temporal response properties. These developmental changes could markedly impact responses to acoustic stimuli throughout the lifetime of the animal.

Methods

Slice Preparation

Auditory thalamocortical slices were prepared from Swiss Webster (SW) or G42 mice (P10–P29) as described by Cruikshank et al. (2002). The G42 line selectively expresses enhanced green fluorescent protein (EGFP) in a subset of parvalbumin expressing (PV+) basket interneurons in strain of CB6 mice (CB6-Tg(Gad1-EGFP)G42Zjh/J; Jackson Laboratories). All surgical procedures followed the guidelines determined by the New York University Animal Welfare Committee. Mice were anesthetized with halothane and decapitated. The brain was exposed, and 2 coronal cuts were made to remove the anterior 25% of the brain and the cerebellum. The brain was then removed from the skull and immersed, anterior cut down, in ice-cold oxygenated (95% O_2–5% CO_2) ACSF (in mM: 125 NaCl, 2.5 KCl, 25 $NaHCO_3$, 1.25 NaH_2PO_4, 1.0 $MgCl_2$, 25 dextrose, and 2 $CaCl_2$) (all chemicals from Sigma). A third cut was made with an ~15° medial to lateral slant to remove the dorsal portion of the brain leaving 1 hemisphere intact. The brain was submerged in ice-cold ACSF, and horizontal slices (300 μm) were made using a vibratome (Campden Instruments). Typically, 1 or 2 slices contained primary auditory cortex (AI), the medial geniculate nucleus (MG), and the thalamocortical fiber tract. The slices were maintained in ACSF at 37 °C for 30 min then rested at room temperature (20–22 °C) for 1–2 h prior to recording (29–33 °C).

Electrophysiology

Neurons were visualized using infrared-differential interference contrast microscopy (IR-DIC) (Olympus). At lower magnification, the MG was visible medial to the hippocampus and posterior to the lateral geniculate nucleus, and AI was located lateral to the anterior half of the hippocampus (see Cruikshank et al. 2002). L2/3 was the cell-dense region 100–300 μm below the pia matter. Only slices containing the MG and AI were used. In a subset of slices, the location of AI was verified by stimulating the MG and recording field potential responses in L3/4. At higher magnification, PCs were identified by a distinct apical dendrite that extended toward L1 while FS cells were distinguished by ovoid somata and multipolar dendrites and, in G42 mice, by GFP fluorescence. Recorded neurons were located 40–70 μm below the slice surface. Whole-cell current-clamp recordings were made simultaneously from up to 4 neurons (amplifier: Dagan Corporation; acquisition and analysis software: Igor Pro; Wavemetrics). Pipettes were pulled from borosilicate glass (2.0 outer diameter) on a Flaming/Brown micropipette puller (Sutter Instruments) to a resistance of 3–10 MΩ. The intracellular solution consisted of (in mM) 130 K-gluconate, 5 KCl, 2 $MgCl_2$, 4 Adenosine triphosphate-Mg, 0.3 Guanine triphosphate, 10 4-(2-hydroxyethyl)-1-piperazineethanesulfonic acid, and 10 phosphocreatine. Voltage clamp recordings were not performed because the standard internal solutions required for adequate space clamp would prohibit the characterization of intrinsic neural properties as well as the ability to assess bidirectional connections.

Stimulation

A series of hyperpolarizing and depolarizing step currents were injected to measure the input resistance, time constant, and suprathreshold properties of each cell. Spike properties were measured for the first spike in the train at rheobase. Spike threshold was the membrane potential that corresponded to the maximum of the second derivative of the membrane voltage between baseline and the peak of the action potential. Spike frequency adaptation was quantified as the ratio of the last interspike interval (ISI_{Last}) to the first (ISI_{First}) in response to a depolarizing step current (1 s) that evoked firing rates of 40 ± 17 Hz. To determine whether pairs of neurons were synaptically connected, 1 neuron was stimulated with 5 suprathreshold current pulses (0.5–1 nA, 5 ms pulse width) delivered at 10 Hz. Average membrane potential responses were compiled from 25 to 35 trials (5 s pause between trials). In connected pairs, postsynaptic potentials (PSPs) that were temporally locked to the presynaptic action potential were evoked in the target cell.

Analysis and Statistics

Presynaptic stimulation successfully evoked an inhibitory postsynaptic potential (IPSP) or excitatory postsynaptic potential (EPSP) if, 1) the onset of PSP was within 3 ms of the presynaptic action potential (AP) initiation; 2) the PSP amplitude (baseline to peak) was a minimum of 0.05 mV; or 3) the PSP peaked within 20 ms (IPSPs) or 7 ms (EPSPs) of onset. Otherwise, the trial was considered a failure with an "amplitude" of 0 mV. The failure rate was determined as the number of failed trials divided by the total number of trials. The reported PSP amplitudes are averaged over all trials and include failures. The reported failure rates, PSP amplitudes, latencies, rise, and decay time constants are for the first PSP in the train. For all PSPs, the amplitude was taken as the difference between the peak of the PSP and the membrane potential at PSP onset. The paired pulse ratio was obtained from the trial-averaged traces and taken as the amplitude of the second PSP divided by the amplitude of the first. For each ensuing PSP, short-term plasticity was determined as the ratio of PSP amplitude relative to the first PSP.

The time constants for the rise (τ_r) and decay (τ_d) of the PSPs were obtained by fitting the normalized (peak − baseline = 1) average PSP, excluding failures, by a difference of 2 exponentials:

$$f\left(t; A, \tau_d, \tau_r\right) = A\left(e^{t/\tau_d} - e^{t/\tau_r}\right). \quad 1$$

Only PSPs that were well fit by equation 1 ($\chi^2 < 1.75$, $n = 155$ EPSPs, $n = 167$ IPSPs) were chosen for analysis. All fits were performed using the Igor Pro, Levenberg-Marquardt nonlinear, least-squares fitting algorithm to search for the coefficient values that minimize chi-squared differences between the fit and data.

All statistics are reported as mean ± standard deviation (SD). Significance was assessed using univariate analysis of variance (ANOVA) with the Tukey's honestly significant difference post hoc test. Homogeneity of variances was confirmed at a <5% level using the Levene's test for homogeneity. The nonparametric Mann–Whitney *U* test was used to assess significance of nonnormally distributed failure rates and for small data sets pertaining to comparisons between successive days in the P19–P29 range. In the latter case, only days with a minimum of 6 samples were tested.

Biocytin Fills

To verify cell identity, 0.5% biocytin was added to the intracellular solution. Slices were fixed in 4% paraformaldehyde for processing. The slices were rinsed with phosphate-buffered saline (PBS), quenched with 1% H_2O_2 in a 10% MeOH–PBS solution, permeabilized in Triton-X-100 and then exposed to avidin–peroxidase complex (ABC kit; Vector Laboratories). The slices were rinsed (with PBS) and reacted with 3,3-diaminobenzidine and then rinsed again. Finally, slices were mounted onto slides with Flourmount for microscopy and cell reconstruction using Neurolucida tracing.

Results

Whole-cell current-clamp recordings were made from 116 FS cells that were synaptically connected to 134 PCs in L2/3 of AI. In both strains of mice, FS cells were identified under IR-DIC by round to ovoid somata with multipolar dendrites. In the G42 mice, the subset of PV+ cells that are FS express the EGFP transgene (Chattopadhyaya et al. 2004) and fluoresce green (Fig. 1*A*, insets). Several neurons ($n = 72$) were filled with biocytin to confirm their identity. We measured the intrinsic

properties of FS cells as well as the synaptic properties of FS–PC pairs from mice ranging in age from P10 to P29. As previously shown for PCs (Oswald and Reyes 2008), both the intrinsic and the synaptic properties of FS cells undergo a transition between P10 and P18 and plateau between P19 and P29. The transitional period was divided arbitrarily into an early phase (P10–P14), which coincides with the critical period for tonotopic map organization in AI of rats (de Villers-Sidani et al. 2007), and a later phase (P15–P18). Between P19 and P29, the values did not significantly differ between successive days (Mann–Whitney *U* test, *P*: 0.07–0.67) or for comparisons of multiple 2- to 4-day subsets in this range (ANOVA *F*: 0.08–2; *P*: 0.14–0.92). All statistical comparisons are between the 3 epochs: P10–P14, P15–P18, and P19–P29.

Developmental Changes in the Intrinsic Properties of FS Interneurons

Typically, FS cells in older animals (P15–P18, P19–P29; Fig. 1, middle, right) have suprathreshold electrophysiological features that distinguish them from PCs and other interneurons (Connors and Gutnick 1990). These include high nonadapting firing rates (ISI_{Last}:ISI_{First}: 1.09 ± 0.14, see Methods), a high rheobase (~0.3), and narrow action potentials (half width, HW: 0.2–0.5 ms), with strong, brief afterhyperpolarizations (τ_{AHP}: 10–50 ms; Fig. 2*A*). FS cells in young animals (P10–P14) did not exhibit these properties (Fig. 1, left). The APs were broader (HW: 0.90 ± 0.30 ms, $P < 0.01$) and taller (42 ± 9 mV, $P < 0.01$) with longer AHPs (τ_{AHP}: 71 ± 49 ms, $P < 0.01$; Fig. 2*A*). The firing rate adaptation ratios were significantly higher (ISI_{Last}:ISI_{First}: 1.4 ± 0.3, $P < 0.01$; Fig. 2*B*) while the firing rates and rheobase values were significantly lower (0.10 ± 0.09 nA, $P < 0.01$). Developmental changes in these properties lead to steeper, right-shifted action potential frequency verses current (F/I) curves in older animals compared with P10–P14 (Fig. 2*C*).

The subthreshold responses of FS cells also varied with age. A series of subthreshold hyperpolarizing and depolarizing current steps were injected to determine the membrane time constant (τ_m) and input resistance (R_n). The τ_m, R_n, and resting membrane potential (V_{rest}) were the highest in neurons between P10 and P14 (τ_m: 23 ± 11 ms; R_n: 294 ± 183 MΩ; V_{rest}: −63 ± 23 mV, $P < 0.01$; Fig. 2*D*,*E* and Table 1). In addition, at P10–P14, there was a prominent sag in response to hyperpolarizing steps (−50 pA, 1 s; Fig. 2*F*, inset) consistent with the presence of I_h (Itami et al. 2007). The amplitude of the sag (the difference between the maximum [step onset] and minimum [step offset] membrane hyperpolarization) was significantly greater between P10–P14 (1.6 ± 1.3 mV) versus P15–P18 (0.3 ± 0.2 mV) or P19–P29 (0.2 ± 0.2 mV; Fig. 2*F*). The mean data and statistics for comparisons between the 3 age groups (P10–P14, P15–P18, and P19–P29) are presented in Table 1.

The identification of FS cells based on electrophysiological properties can be difficult particularly in young animals (P10–P14) since "FS" responses are less apparent. Since the majority of FS interneurons are PV+ (Kawaguchi and Kondo

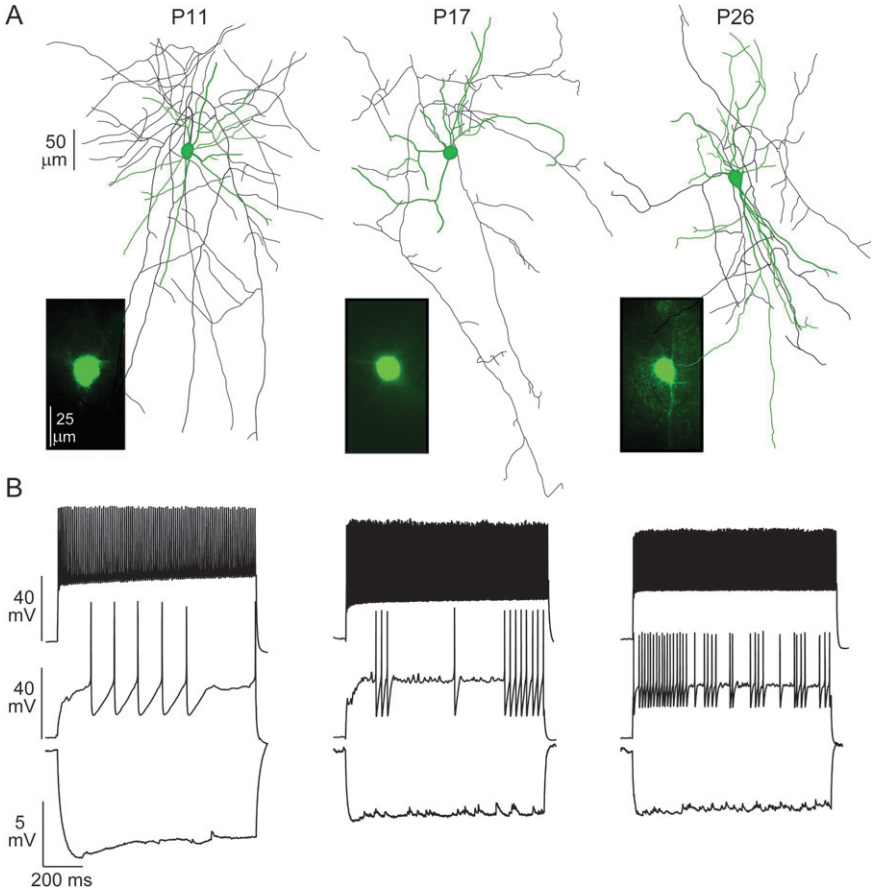

Figure 1. Development of FS characteristics. (*A*) Representative GFP+ (insets) FS cells recorded in G42 mice at P11, P17, and P26. The neurons were also filled with biocytin for reconstruction of dendritic (green) and axonal arbors (black). (*B*) The responses of the corresponding neurons in (*A*) to hyperpolarizing (−0.05 nA, lower), near rheobase (0.1–0.5 nA, middle) and strongly depolarizing (0.5–1.0 nA, upper) current step injections.

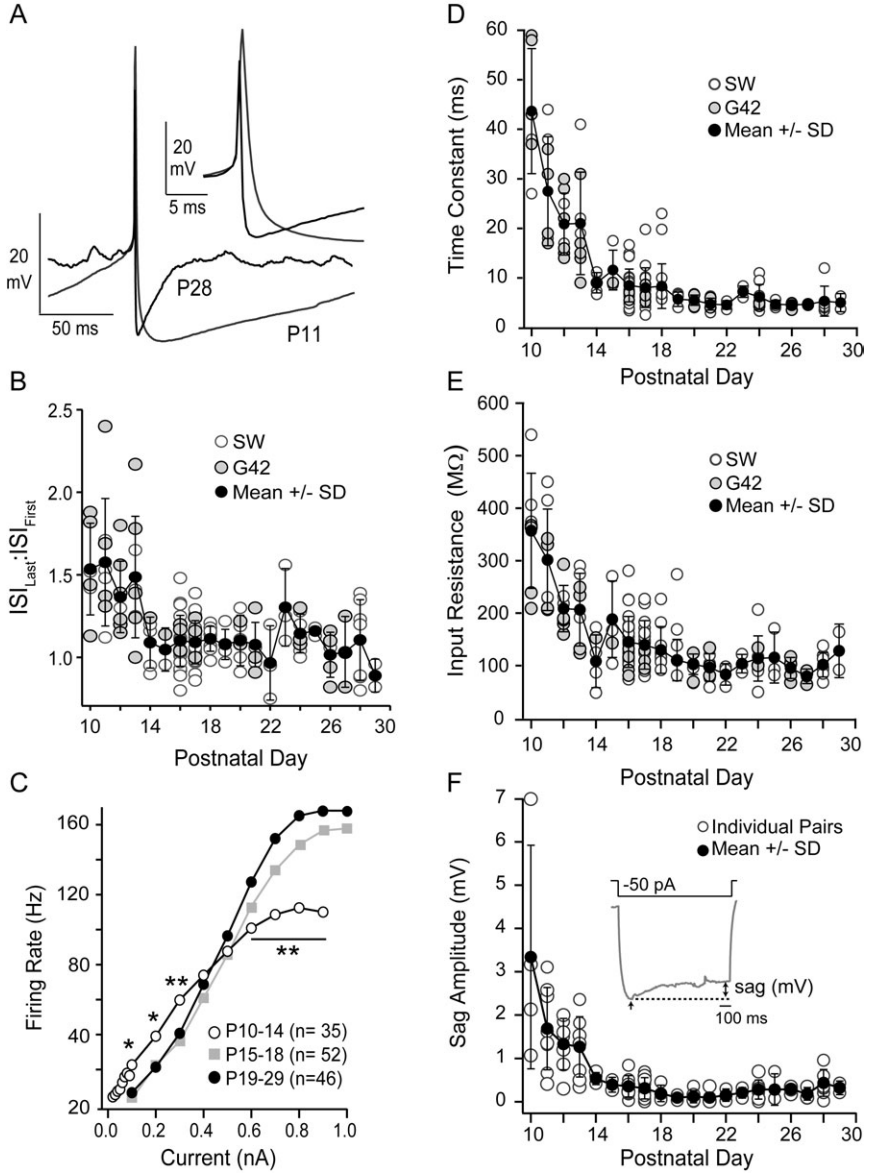

Figure 2. Development of intrinsic membrane properties. (*A*) Single-action potentials recorded at P11 (gray) and P28 (black) aligned at threshold (arrow) to show the age-dependent differences in spike properties. The spike width (inset) and duration of the AHP decrease significantly with age. (*B*) The adaptation ratio (ISI_{Last}:ISI_{First}, mean ± SD, black circles) decreases significantly with age in G42 (gray circles) and SW (open circles). (*C*) The average firing rate (hertz) versus injected current for FS cells recorded at P10–P14 (white circles), P15–P18 (gray squares), and P19–P29 (black circles). The firing rates for low (0.1–0.3 nA), and high (0.6–0.9 nA) input currents in P10–P14 neurons differed significantly from older animals (*$P < 0.05$; **$P < 0.01$). (*D*) Membrane time constants of FS cells versus postnatal day age in SW mice (open circles) and G42 mice (gray circles). The mean ± SD (black circles) over all neurons for each day is also plotted. (*E*) The input resistances of FS cells versus postnatal day age (symbols as in *D*). The membrane time constants and input resistances did not differ between strains of mice (see Supplementary Table 1 for comparison of SW and G42 strains). Over all neurons, the time constants and input resistances decreased significantly with age (see Table 1). (*F*) The amplitude of sag versus postnatal day age. Inset: the sag response to a 1-s −50 pA step current injection at P11. The amplitude of the sag (millivolt) was the difference (double-headed arrow) between the average steady state hyperpolarization during the last 100 ms of the step and the maximum hyperpolarization (single-headed arrow) at the onset of the step. In all plots, the error bars are SD.

2002) and G42 mice express the EGFP transgene in (PV+) cells, we compared the properties of GFP+ interneurons recorded from G42 mice with FS cells recorded in SW mice of the same age. We found that the intrinsic membrane properties and AP properties (Fig. 2 and Supplementary Table 1) of the FS cells in our dataset did not differ between G42 and SW mice at any age.

Characterization of PSPs

The synaptic properties of younger animals, P10–P14 and P15–P18, significantly differed from those at the steady state, P19–P29. The statistics of the synaptic properties for the 3 age groups are presented in Tables 2 and 3.

Excitatory Connections between PC and FS Cells

The mean and variability of EPSP amplitudes at PC-to-FS synapses decreased significantly between P10–P14 (1.8 ± 1.6 mV) and P19–P29 (1.1 ± 0.9 mV, $P < 0.01$; Fig. 3*A*). Over all ages, the mean amplitude was correlated with the input resistance (R: 0.60, $P < 0.01$; data not shown). These synapses were highly reliable with only a small but significant increase in the failure rate of the first EPSP with age (P10–P14—mean:

Table 1
Intrinsic properties of FS cells from P10 to P29

Age	P10–P14; $n = 36$	P15–P18; $n = 59$	P19–P29; $n = 50$	F value	P value
R_n (MΩ)	266 ± 139	141 ± 50**	103 ± 30*††	50	4.7×10^{-17}
τ_m (ms)	25 ± 14	8 ± 4**	5 ± 2††	81	3.0×10^{-24}
V_{rest} (mV)	−65 ± 6	−72 ± 4**	−70 ± 5††	34	1.5×10^{-13}
V_{thresh}	−37 ± 6	−33 ± 5**	−35 ± 6	4.4	0.011
Rheobase (nA)	0.10 ± 0.10	0.27 ± 0.10**	0.33 ± 0.13**††	48	1.5×10^{-16}
AP amplitude (mV)	42 ± 9	32 ± 9**	30 ± 9††	15	1.3×10^{-6}
HW (ms)	0.9 ± 0.3	0.5 ± 0.2**	0.3 ± 0.1**††	95	3.6×10^{-26}
AHP (mV)	18 ± 3	18 ± 3	16 ± 3*†	5.4	0.006
τ_{AHP} (ms)	71 ± 50	39 ± 21**	18 ± 7*††	23	9.6×10^{-9}
ISI_L/ISI_1	1.4 ± 0.3	1.1 ± 0.1**	1.1 ± 0.2††	34	1.4×10^{-12}
Sag	1.6 ± 1.3	0.3 ± 0.2**	0.2 ± 0.2††	32	2.5×10^{-11}

Note: Since the properties of FS cells did not differ between SW and G42 mice, the mean and SD of the intrinsic membrane and action potential properties over all neurons are presented. Abbreviations: R_n, input resistance; τ_m, membrane time constant; V_{rest}, resting membrane potential; V_{thresh}, threshold membrane potential; HW, action potential width at half maximum; ISI_L/ISI_1, adaptation ratio. Significance at $^{**}P < 0.01$, $^{*}P < 0.05$ with column to immediate left (i.e., P10–P14 vs. P15–P18 and P15–P18 vs. P19–P29), $^{††}P < 0.01$, $^{†}P < 0.05$ for P10–P14 versus P19–P29. F values and P values are for ANOVA comparisons between multiple age groups.

Table 2
Summary of developmental changes in excitatory synaptic properties

Age	P10–P14; $n = 27$	P15–P18; $n = 89$	P19–P29; $n = 55$	F value	P value
Latency (ms)	1.0 ± 0.3	1.1 ± 0.5	0.9 ± 0.3*	5.3	0.034
τ_r (ms)	1.4 ± 0.6	1.4 ± 0.6	1.2 ± 0.7	2.5	0.082
τ_d (ms)	37 ± 26	20 ± 9**	15 ± 8††	2.7	5×10^{-11}
t_{peak} (ms)	6 ± 2	6 ± 2	5 ± 2	3.0	0.053
Amplitude (mV)	1.8 ± 1.6	1.3 ± 1.2	1.1 ± 0.9†	3	0.047
Fail rate	0.10 ± 0.13	0.14 ± 0.14	0.14 ± 0.16†	n/a	n/a
PPR	0.4 ± 0.1	0.7 ± 0.2**	0.8 ± 0.2††	22	2.6×10^{-9}
V_m (mV)	−66 ± 6	−73 ± 4**	−73 ± 4††	33	6.5×10^{-13}

Note: τ_r, EPSP rise constant; τ_d, EPSP decay constant; t_{peak}, time to peak from onset; n/a, not applicable; PPR, paired pulse ratio; V_m, membrane potential at which PSPs were recorded. Significance at $^{**}P < 0.01$, $^{*}P < 0.05$ with column to immediate left (i.e., P10–P14 vs. P15–P18 and P15–P18 vs. P19–P29), $^{††}P < 0.01$, $^{†}P < 0.05$ for P10–P14 versus P19–P29. F values and P values are for ANOVA comparisons between multiple age groups. ANOVA was n/a for statistical analysis of synaptic failure rate.

Table 3
Summary of developmental changes in inhibitory synaptic properties

Age	P10–P14; $n = 26$	P15–P18; $n = 97$	P19–P29; $n = 65$	F value	P value
Latency (ms)	0.8 ± 0.4	0.9 ± 0.3	0.6 ± 0.3**††	11	2.0×10^{-5}
τ_r (ms)	6 ± 3	4 ± 1**	3 ± 1**††	14	1.6×10^{-6}
τ_d (ms)	68 ± 34	54 ± 30	50 ± 31†	3.4	0.04
t_{peak} (ms)	16 ± 5	13 ± 3**	13 ± 4††	12	1.3×10^{-5}
Amplitude (mV)	0.8 ± 0.5	0.7 ± 0.2	0.5 ± 0.3*††	6.9	1.0×10^{-3}
Fail rate	0.12 ± 0.12	0.11 ± 0.14	0.14 ± 0.14	n/a	n/a
PPR	0.7 ± 0.2	0.7 ± 0.2	0.7 ± 0.2	2.7	0.07
V_m (mV)	−59 ± 5	−61 ± 3	−61 ± 3	0.93	0.4

Note: τ_r, IPSP rise constant; τ_d, IPSP decay constant; t_{peak}, time to peak from onset; n/a, not applicable; PPR, paired pulse ratio; V_m, membrane potential at which PSPs were recorded. Significance at $^{**}P < 0.01$, $^{*}P < 0.05$ with column to immediate left (i.e., P10–P14 vs. P15–P18 and P15–P18 vs. P19–P29), $^{††}P < 0.01$, $^{†}P < 0.05$ for P10–P14 versus P19–P29. F values and P values are for ANOVA comparisons between multiple age groups. ANOVA was n/a for statistical analysis of synaptic failure rate.

0.08 ± 0.13, median: 0.0; P15–P18 and P19–P29—mean: 0.14 ± 0.14, median: 0.09, $P < 0.05$, Mann–Whitney U test).

PC–FS synapses showed frequency-dependent short-term depression that decreased with age (Fig. 3*B–D*). The paired pulse ratios (10-Hz stimulation; PPR = $EPSP_2/EPSP_1$) indicated that P10–P14 synapses were significantly more depressed (PPR: 0.4 ± 0.1) than either P15–P18 (0.7 ± 0.2) or P19–P29 (0.8 ± 0.2). At higher stimulation frequencies (20 and 40 Hz), P19–P29 synapses showed significantly less paired pulse depression (Fig. 3*D*) compared with synapses between P10 and P18. To assess the ability of synapses to follow repetitive stimuli, we calculated the ratio of the fifth EPSP to the first EPSP. EPSPs between P10 and P14 exhibited the most attenuation by the fifth pulse at all stimulation frequencies, while P19–P29 EPSPs showed the least attenuation (Fig. 3*E*). This suggests that the ability of PC–FS synapses to follow repetitive inputs is enhanced with age.

Next, we measured the temporal properties of the EPSPs at different ages. The EPSP latency, defined as the time difference between the onset of the EPSP and the onset of the presynaptic AP, decreased with age between P15–P18 (1.1 ± 0.5 ms) and P19–P29 (0.9 ± 0.3 ms, $P < 0.05$) (Table 2). However, the time-to-peak (t_{peak}), taken as the difference between the maximum of the EPSP and onset, was 6 ± 2 ms and did not change (Table 2). There was also a significant change in the decay of the EPSP that decreased the duration of the EPSPs with age (Fig. 3*F*). To obtain the time constants for the rise (τ_r) and decay (τ_d) of the EPSP, the average EPSP for each pair was fit with a difference of 2 exponentials (see Methods). Although τ_r did not change with age (1.4 ± 0.9 ms, Table 2), the decay of the EPSP (τ_d) decreased significantly between P10–P14 (37 ± 26 ms) and P19–P29 (16 ± 8 ms, $P < 0.01$) (Fig. 3*G*). These age-dependent decreases in τ_d may, in part, be attributed to changes in the membrane time constant of the FS cells since the mean τ_d and τ_m at each age were linearly correlated (R: 0.88, $P < 0.01$, Fig. 3*H*). In addition, at resting membrane potentials, the EPSPs were completely blocked by α-amino-3-hydroxyl-5-methyl-4-isoxazole-propionate (AMPA) receptor antagonist, DNQX ($n = 8$; ages P14, P17, P18, and P22; Fig. 3*I*). These results suggest that τ_m and AMPA receptor kinetics dominate the synaptic time course at rest but do not preclude the possibility that the dynamics of NMDA receptors contribute at higher membrane potentials.

Inhibitory Connections between PC and FS Cells

There were significant developmental changes in the IPSPs. The measured synaptic parameters did not differ between SW mice and G42 mice (see Supplementary Table 2). IPSP amplitudes decreased from 0.8 ± 0.5 mV (P10–P14) to 0.5 ± 0.3 mV (P19–P29, $P < 0.01$; Fig. 4*A*,*B* and Table 3). The decrease in mean input resistance of the postsynaptic PC was correlated with mean IPSP amplitude (R: 0.77, $P < 0.01$; Fig. 4*C*) and thus may contribute to changes in IPSP amplitudes. The IPSP amplitudes were not influenced by changes in Cl^- driving force because the PCs were held at approximately –60 mV (Table 3), and the intracellular solution sets the Cl^- reversal potential to approximately –72 mV. Consequently, there was no correlation between IPSP amplitude and membrane potential (R: –0.19; data not shown). Representative IPSPs for each age group are shown in Figure 4*D*. Inhibitory responses evoked with single-stimulus pulses were completely blocked by the γ-aminobutyric acid A ($GABA_A$) receptor antagonist bicuculline (10 μM; Fig. 4*E*, $n = 16$). We have shown previously that high frequency (40–80 Hz) multipulse (10–20) stimulation evokes bicuculline insensitive, $GABA_B$ responses that do not vary with age (Oswald et al. 2009).

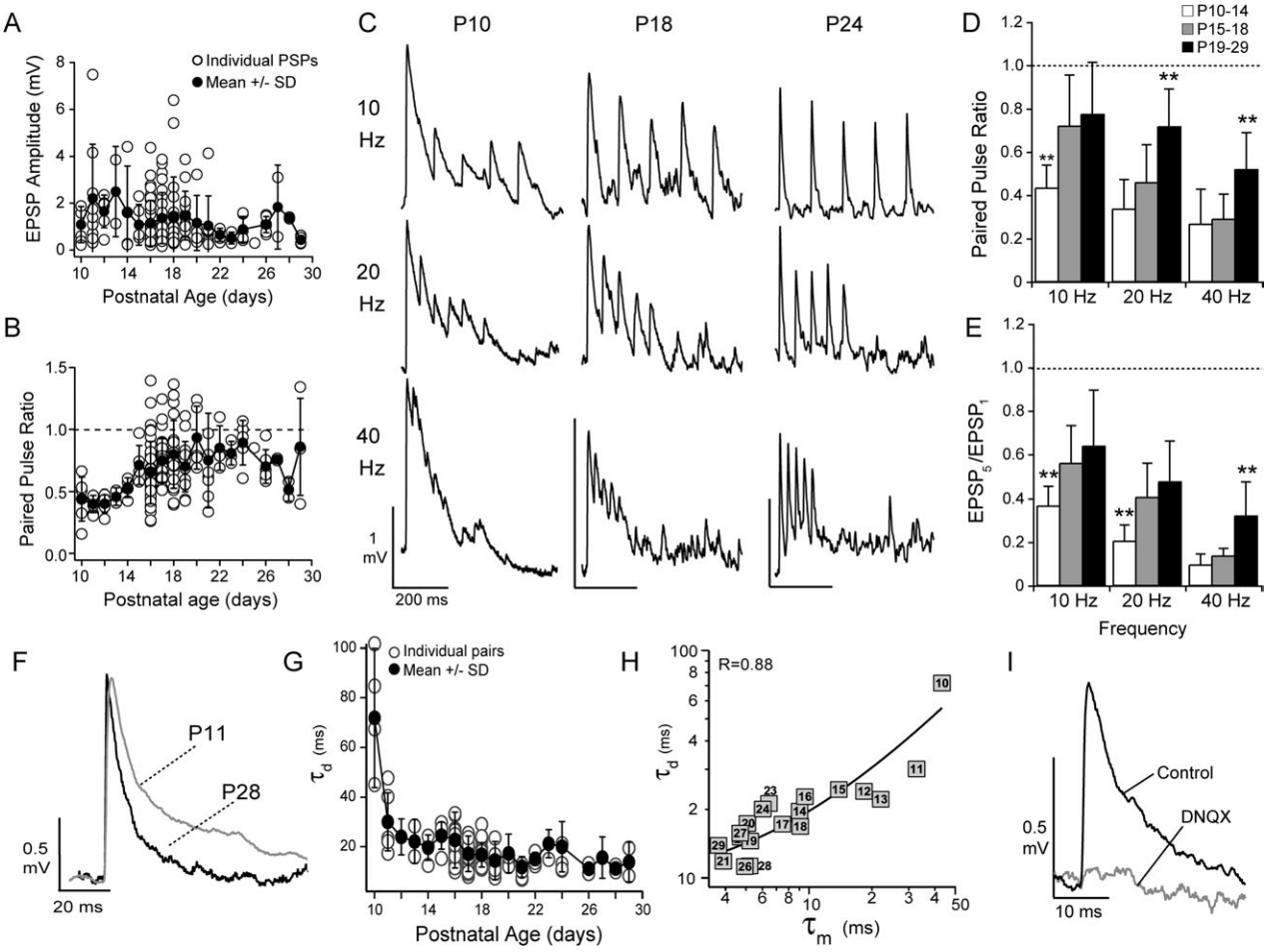

Figure 3. Properties of excitatory synaptic potentials to FS cells. (*A*) The mean ± SD (black circles) EPSP amplitude decreased with postnatal day age in PC to FS pairs (open circles). (*B*) The paired pulse ratio (10-Hz stimulation) increases with postnatal day age (symbols as in *A*). (*C*) Sample traces in response to 10-, 20-, and 40-Hz stimulation of the presynaptic PC at P10, P18, and P24. (*D*) The average paired pulse ratios for 10-, 20-, and 40-Hz stimulation over the 3 age groups P10–P14 (white bars), P15–P18 (gray bars), and P19–P29 (black bars). The P10–P14 neurons showed the significantly stronger paired pulse depression at 10 Hz (white bars, $^{**}P < 0.01$) compared with the other age groups. The P19–P29 neurons showed the least depression (black bars, $^{**}P < 0.01$) at higher stimulus frequencies (20 and 40 Hz). (*E*) The ratio of the amplitude of the fifth EPSP in the train to the first EPSP in the trains for the 3 age groups. For 10- and 20-Hz stimulation, P10–P14 neurons (white bars) showed the most depression while P19–P29 neurons showed the least depression at 40 Hz (black bars, $^{**}P < 0.01$). (*F*) Representative EPSPs recorded at P11 (gray) and P28 (black). (*G*) EPSP amplitudes were normalized to 1 and the EPSPs were fit by a difference of 2 exponentials to obtain time constants for the rise (τ_r) and decay (τ_d). The τ_d decreased with postnatal day age (open circles). Filled circles are the mean ± SD for each age. (*H*) The mean τ_d was positively correlated with membrane time constant (τ_m) for each postnatal day (denoted by numbered boxes) (*R*: 0.88, linear fit, black line). (*I*) The EPSPs (black) were completely blocked by the AMPA receptor antagonist DNQX (20 μM, gray, $n = 8$) at resting membrane potentials (−65 to −75 mV).

Inhibitory synapses had low failure rates (0.12 ± 0.14, median: 0.077) and exhibited moderate paired pulse depression (PPR: 0.7 ± 0.2) that did not vary significantly with age or stimulation frequency (Fig. 4*F,G* and Table 3). The $IPSP_5/IPSP_1$ ratio did decrease with frequency between 10 Hz (0.56 ± 0.16) and 20 Hz (0.36 ± 0.19, $P < 0.01$) or 40 Hz (0.29 ± 0.13, $P < 0.01$; Fig. 4*H*) but did not change with age.

The time course of the IPSPs decreased with age (Fig. 5*A* and Table 3). The IPSP latency was significantly shorter at P19–P29 (0.6 ± 0.3 ms) than P10–P14 (0.8 ± 0.4 ms, $P < 0.05$) or P15–P18 (0.9 ± 0.3 ms, $P < 0.01$; Fig. 5*B*). The time to reach maximum hyperpolarization (t_{peak}) was significantly shorter at P15–P18 (13 ± 0.3 ms) and P19–P29 (13 ± 0.4 ms) versus P10–P14 (16 ± 5 ms, $P < 0.01$; Fig. 5*C*). Likewise, the time constants to reach maximum hyperpolarization and then return to rest, termed rise (τ_r) and decay (τ_d), respectively, for convenience, decreased with age (τ_r—P19–P29: 3 ± 2 ms vs. P15–P18: 4 ± 1 ms, $P < 0.05$, or P10–P14: 6 ± 3, $P < 0.01$; τ_d—P19–P29: 50 ± 31 ms, P10–14: 68 ± 34, $P < 0.05$; Fig. 5*D*,E, left). Finally, both the mean τ_r and τ_d were linearly correlated with the mean τ_m of the PC at each age (*R*: 0.80, *R*: 0.83, respectively, $P < 0.01$; Fig. 5*D*,*E*, right).

Differential Synaptic Properties between PC–PC and PC–FS Pairs

In Figure 6 we compare the development of the temporal synaptic properties of PC-to-PC (Oswald and Reyes 2008), PC-to-FS, and FS-to-PC connections for each age group (P10–P14, P15–P18, and P19–P29). The IPSP latencies, rise, and peak times decreased significantly between P10–P14 and P19–P29 (white asterisks on black bars, Fig. 6*A–C*), whereas these properties, with the exception of PC–FS latency, did not vary at excitatory synapses between P10 and P29. All synapses showed age-dependent decreases in synaptic decay (Fig. 6*D*)—PC–FS connections reached steady-state values by P15–P18 (white asterisks, gray bar) while FS–PC and PC–PC connections reached steady state at P19–P29 (white asterisks, black bars). With the exception of latency, inhibitory synaptic timescales—the rise, peak and decay of the IPSP—were significantly longer

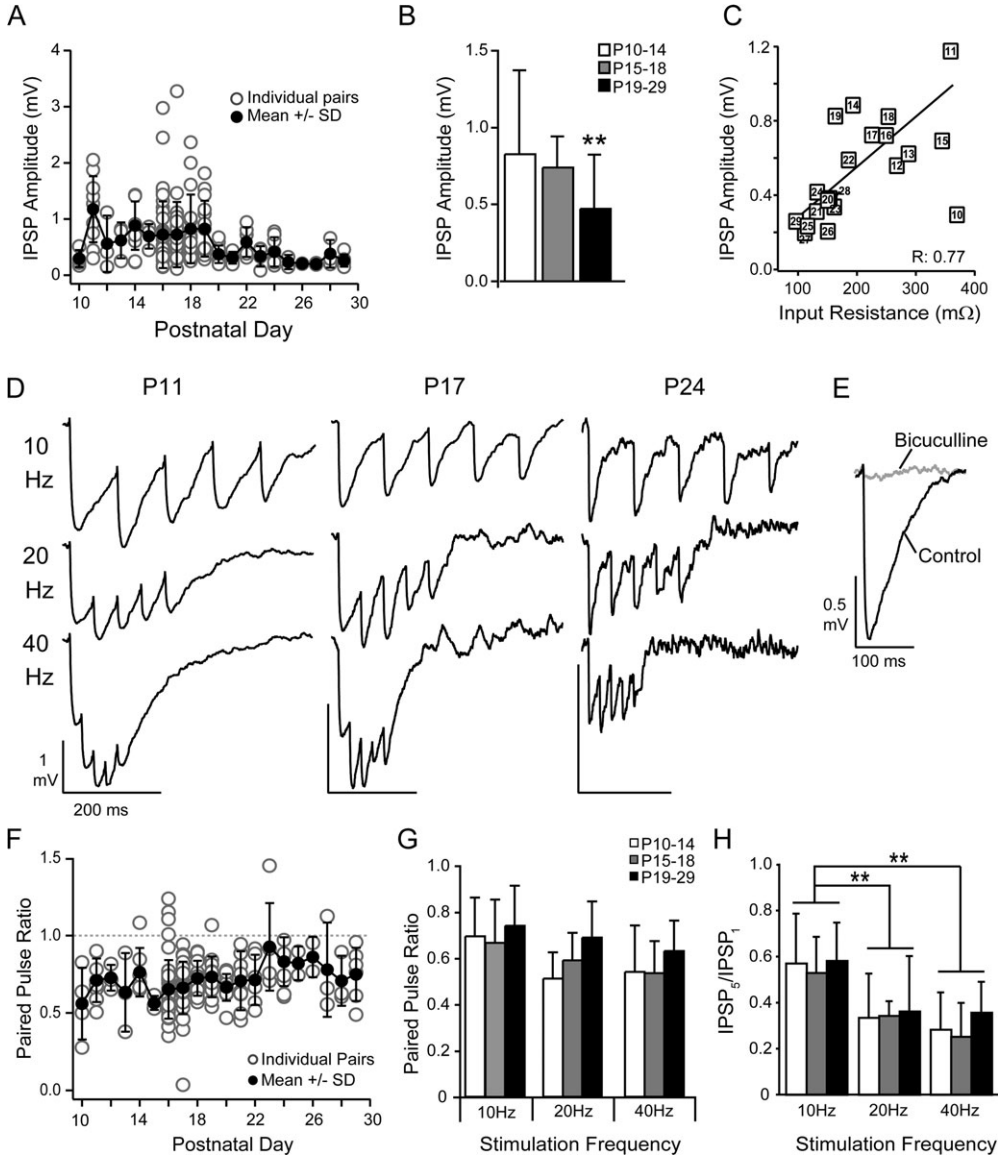

Figure 4. Developmental changes in inhibitory synaptic potentials. (*A*) The mean ± SD (black circles) IPSP amplitudes decrease with postnatal day age. Open circles are amplitudes for individual pairs. (*B*) The average IPSP amplitudes for the 3 age groups (P10–P14, P15–P18, and P19–P29). The IPSP amplitudes significantly decreased at P19–P29 versus P10–P14 (**$P < 0.01$). (*C*) IPSP amplitudes were correlated (*R*: 0.77) with changes in input resistance in the postsynaptic PCs (number in symbol indicates postnatal day). (*D*) Sample traces in response to 10-, 20-, and 40-Hz stimulation of the presynaptic FS cell at P11, P17, and P24. (*E*) The inhibitory response was completely blocked by 10 μM bicuculline. (*F*) The paired pulse ratio (10 Hz) did not change with postnatal day (symbols as in *A*). (*G*) The average paired pulse ratios for 10-, 20-, and 40-Hz stimulation over the 3 age groups P10–P14 (white bars), P15–P18 (gray bars), and P19–29 (black bars). (*H*) The ratio of the amplitude of the fifth IPSP in the train to the first EPSP in the trains for the 3 age groups. There was significant depression of the fifth pulse at higher frequencies (**$P < 0.01$) but this was independent of age.

than excitatory timescales (FS–PC connections; open stars, Fig. 6*B–D*). Although the latency of PC–PC synapses was significantly longer than PC–FS or FS–PC synapses at all ages ($P < 0.01$), the onset of inhibition is subject to latencies in PC–FS and FS–PC synapses as well as the time to integrate PC–FS drive. Taken together, these results suggest that the development of the temporal properties that influence the onset of inhibition lag those of excitation and that the slower timescales of inhibition limit temporal processing throughout development.

Discussion

The influence of inhibition during auditory processing depends on at least 3 factors: 1) the intrinsic excitability of the interneurons, 2) the strength and timing of the excitatory drive to the interneurons, and 3) the strength and timing of inhibitory synaptic input. We find that all these factors change during early development of L2/3 FS–PC circuits in AI.

Development of Intrinsic Properties in FS Interneurons

The age-related changes in the intrinsic properties of FS cells are similar to the developmental profile of L2/3 PCs in AI (Oswald and Reyes 2008) and are comparable to previous studies of interneurons in AI (Metherate and Aramakis 1999) and other cortical areas (Itami et al. 2007; Doischer et al. 2008; Okaty et al. 2009). In young animals, high input resistance, depolarized membrane potentials, and lower AP thresholds increase FS cell excitability, while broad APs, long AHPs, and

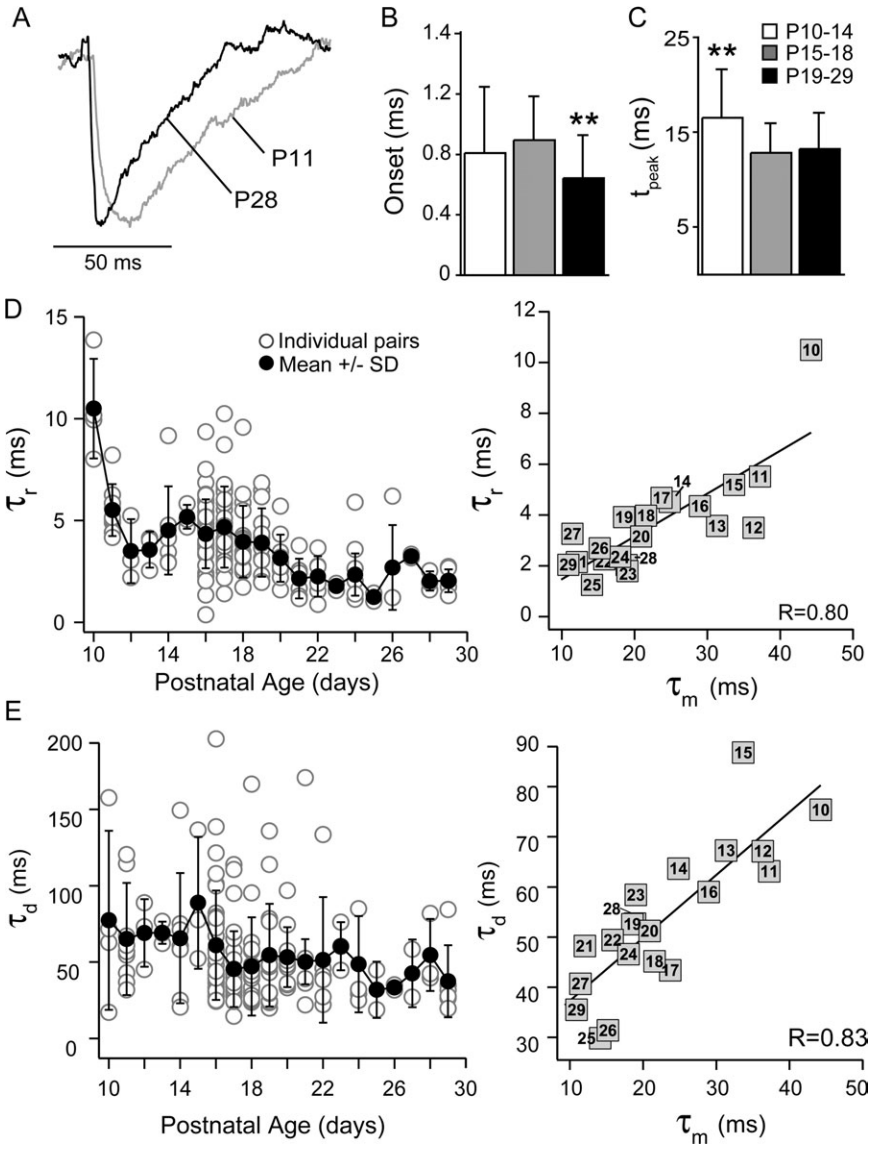

Figure 5. Temporal properties of IPSPs. (*A*) Representative IPSPs recorded at P11 (gray) and P28 (black). (*B*) The IPSP onset latencies were significantly shorter at P19–P29 (black bars) than at P10–P14 (white bars) or P15–P18 (gray bars) (**$P < 0.01$). (*C*) The time from the IPSP onset to peak was significantly longer in P10–P14 animals (**$P <$ 0.01). IPSP amplitudes were normalized to 1 and the IPSPs were fit by a difference of 2 exponentials to obtain time constants for the rise (τ_r) and decay (τ_d). (*D*) Left: The τ_r decreased with postnatal day age (mean ± SD, black circles; individual pairs, white circles). Right: The mean τ_r was positively correlated with the membrane time constant (τ_m) of the postsynaptic PC for each postnatal day (*R*: 0.80, black line). (*E*) Left: The τ_d decreased with postnatal day age (symbols as in *D*) Right: The mean τ_d was positively correlated with the τ_m of the postsynaptic PC for each postnatal day (*R*: 0.83, black line).

high adaptation ratios lower overall firing rates. In older animals, neural excitability and spike frequency adaptation ratios decreased, which was manifested as a rightward shift of the F/I curve and higher firing rates. These changes coincide with the early development (P7–P25) of potassium channels in PV+ FS cells that contribute to leak (Kcnk3 and Kcnk1) and spike repolarization (Kv3 and Kcnn2) (Du et al. 1996; Rudy and McBain 2001; Tansey et al. 2002; Okaty et al. 2009). The developmental changes in these intrinsic properties suggest that FS cell precision in spike timing improves with age (Doischer et al. 2008).

In addition to spike responses, the changes in intrinsic properties can also contribute to synaptic responses. The decreases input resistance and membrane time constants in both FS cells and PCs (Oswald and Reyes 2008) throughout early development influence the strength and time course of PSPs in the FS–PC network. This may further impact the timing of inhibition with respect to excitation during the processing of acoustic information.

Development of Synaptic Properties

In other sensory cortices, EPSPs between PC–FS cell pairs are strong and reliable and exhibit significant short-term depression (Markram et al. 1998; Reyes et al. 1998; Holmgren et al. 2003). In AI of animals younger than P18, approximately 20% of pairs have EPSP amplitudes between 2 and 8 mV, which suggest that fewer inputs may be required to drive FS cells as has been suggested for PC–PC pairs (Lefort et al. 2009). However, by P19–P29, amplitudes greater than 2 mV are rarely observed. At rest, the short duration EPSPs are consistent with

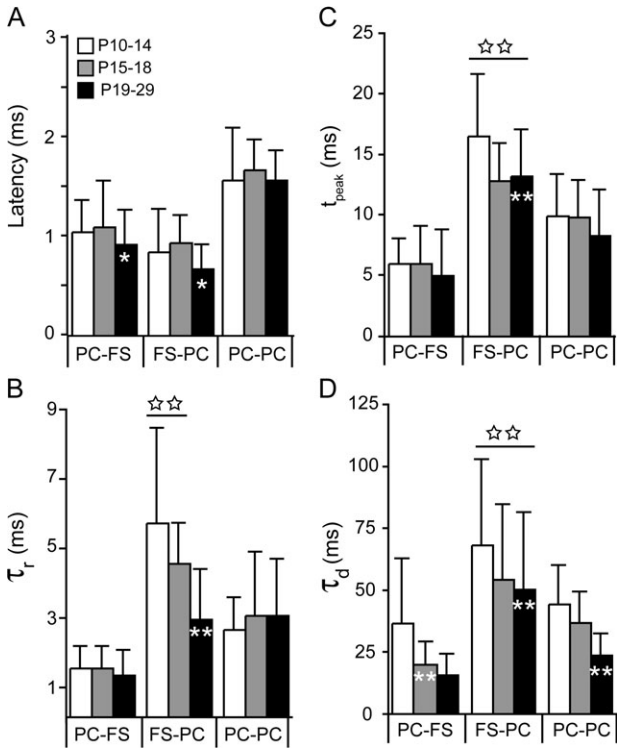

Figure 6. Comparison of temporal synaptic properties between PCs and FS interneurons. The temporal properties of EPSPs between PC–PC pairs (white bars, Oswald and Reyes 2008) and PC–FS pairs (black bars) as well as IPSPs between PC–FS pairs (gray bars) are shown for each age group (P10–P14, P15–P18, and P19–29). White asterisks on the bars represent statistically significant changes with age, while significant differences between inhibitory synapses and excitatory synapses are indicated by open stars above the bars. All data are presented as mean ± SD, and statistical significance was assessed with ANOVA, where $*P < 0.05$ and double asterisks or double stars are $P < 0.01$. (*A*) PSP latency is defined as the difference between the onset of the PSP and the onset of the presynaptic action potential. IPSP latencies decreased with age as did PC–FS EPSP latencies (white asterisk, black bar). The EPSP latencies in PC–PC pairs did not change with age but had the longest latencies at all ages compared with other connections ($P < 0.01$). (*B*) The rise time constants (τ_r) of the IPSPs decreased with age (white asterisk, black bar) and were significantly longer at young ages (P10–P14 and P15–P18) than those of the EPSPs at any age (double stars). (*C*) The time-to-peak (measured from PSP onset) did not change for EPSPs but decreased with age for IPSPs (white double asterisks). In addition IPSPs in younger neurons had the longest peak times (double open stars). *D*) The time constant of decay (τ_d) of all synapses decreased with age (white double asterisks). At all ages, the IPSP decays are significantly longer than EPSPs (open stars).

predominantly AMPA receptor–mediated current and correlated with FS cell membrane time constants throughout development. However, our results do not preclude the possibility that developmental changes in AMPA and/or NMDA receptor composition (Lambolez et al. 1996; Kumar et al. 2002; Lu et al. 2007; Wang and Gao 2009) may also contribute to synaptic decays at higher resting potentials than we report. These decreases in EPSP amplitude and duration suggest that increased synchrony in PC inputs may be required to drive FS cells in older animals.

The strength and temporal properties of inhibitory synaptic inputs also changed significantly with age. The rise, peak, and decay times of the IPSPs decreased with age, which may, in part, be attributed to correlated decreases in membrane time constant of the postsynaptic PCs. However, the developmental transition from slow α_3 subunits in $GABA_A$ receptors to faster α_1 subunits may also contribute to changes in IPSP rise and decay times (Gingrich et al. 1995; Xu et al. 2010). There is also a modest but significant decrease in IPSP amplitude between P10 and P29. These results were somewhat unexpected given that IPSC amplitudes in other cortical areas increase with age (Doischer et al. 2008; Kobayashi et al. 2008); α_1 $GABA_A$ receptor subunits have a higher peak current than α_3 subunits (Gingrich et al. 1995) and GAD65 expression increases (Xu et al. 2010). Alternatively, recent in vivo studies in AI have shown that inhibitory strength is stable throughout early development (Dorrn et al. 2010; Sun et al. 2010). One likely explanation for our results is that correlated decreases in PC input resistance during development counter increases in IPSC amplitude. It remains to be determined how changes in inhibitory strength between pairs of neurons are reflected at the population level in vivo.

Implications for Auditory Processing During Development

The majority of in vivo studies have focused on development of the thalamorecipient layers in AI. Although the maturation L2/3 of acoustically evoked auditory responses has yet to be fully elucidated, it is plausible that many of the mechanisms that underlie cortical development in L3–L5 are comparable to those in L2/3. Adult L2/3 neurons are tuned to both pure tones and more complex sustained auditory inputs (Volkov and Galazjuk 1991; Ojima and Murakami 2002; Wang et al. 2005), process binaural inputs (Ojima and Murakami 2002), and participate in oscillatory activity (Barth and MacDonald 1996). Since PC and FS cells in L2/3 are highly interconnected (Oswald et al. 2009), FS cells are a major source of inhibition in the superficial layers. Thus, the development of FS–PC inhibition can influence both feed-forward processing such as tuning and recurrent processing during repetitive, sustained, or oscillatory activity. It has been suggested that the establishment of inhibitory tuning lags excitatory tuning (Chang et al. 2005; Dorrn et al. 2010; but also see Sun et al. 2010). We have shown that the temporal properties of EPSPs mature earlier than those of IPSPs (Fig. 6; Oswald and Reyes 2008). This may contribute to establishing excitatory responses early in development, which are then refined by feed-forward and recurrent inhibition as the animal matures.

Inhibition is often mediated through a disynaptic circuit that results in IPSPs that are slightly delayed with respect to EPSPs (Wehr and Zador 2003; Tan et al. 2004, 2007; Wu et al. 2006, 2008). The timescales of this EPSP–IPSP sequence set the duration of the integration window. We have shown that IPSPs peak later in P10–P14 neurons than in P19–P29 neurons. This would likely decrease overlap between EPSPs and IPSPs, broaden the integration window in young animals, and allow spike responses to nonoptimal or less precisely timed inputs. As AI develops, IPSP rise, peak, and decay times decrease, as do the decays of PC–PC EPSPs. This increases the overlap between excitation and inhibition and shortens integration windows. Comparable changes in integration window have been shown to impact the tuning of spiking responses to acoustic stimuli in L3 neurons in AI (Ojima and Murakami 2002) and may also increase the precision of spiking during development (Dorrn et al. 2010).

The recruitment of inhibition may also influence cortical responsiveness during masking, repetitive, or oscillatory activity. We have shown that the decay constants of inhibitory synapses were significantly longer than excitation at all ages.

This suggests that inhibition sets an upper frequency bound for responses to inputs arriving at short intervals. In young animals, IPSPs are approximately 60–200 ms long and can summate during repetitive (Fig. 5) or asynchronous stimulation producing long-lasting hyperpolarizations that reduce responsiveness to frequencies >10 Hz. In older animals, decreased IPSP durations (25–50 ms) limit summation and increase neural responsiveness to higher input frequencies (20–40 Hz). Finally, the decreases in short-term synaptic depression at excitatory synapses suggest that the recruitment of both excitation and inhibition during repetitive stimulation improves with age. This combined with narrower integration windows suggests that phase locking, the ability to respond to repetitive stimuli, and oscillatory frequencies are increased in L2/3 during development.

In closing, the results of this and our companion study (Oswald and Reyes 2008) suggest that the developmental changes in the intrinsic and synaptic properties of PC–FS circuitry lead to faster timescales that can enhance precision and temporal responsiveness of neurons in L2/3. Further in vivo studies are necessary to elucidate functional implications of the maturation of these circuit properties during auditory processing.

Supplementary Material

Supplementary material can be found at: http://www.cercor.oxfordjournals.org/.

Funding

National Institutes of Health (DC005787-01A1 to A.D.R.); the Robert Leet and Clara Guthrie Patterson Trust Postdoctoral Fellowship in Brain Circuitry (to A.M.O.).

Notes

We thank A. Takesian for helpful comments. *Conflict of Interest*: None declared.

References

Atallah B, Scanziani M. 2009. Instantaneous modulation of gamma oscillation frequency by balancing excitation with inhibition. Neuron. 62:566–577.

Barbour D, Callaway EM. 2008. Excitatory local connections of superficial neurons in rat auditory cortex. J Neurosci. 28:11174–11185.

Barth DS, MacDonald KD. 1996. Thalamic modulation of high-frequency oscillating potentials in auditory cortex. Nature. 383:78–81.

Beierlein M, Gibson JR, Connors BW. 2003. Two dynamically distinct inhibitory networks in layer 4 of the neocortex. J Neurophysiol. 90:2987–3000.

Brosch M, Budinger E, Scheich H. 2002. Stimulus-related gamma oscillations in primate auditory cortex. J Neurophysiol. 87:2715–2725.

Brosch M, Schreiner CE. 1997. Time course of forward masking tuning curves in cat primary auditory cortex. J Neurophysiol. 77:923–943.

Chang E, Bao S, Imaizumi K, Schreiner CE, Merzenich MM. 2005. Development of spectral and temporal response selectivity in the auditory cortex. Proc Natl Acad Sci U S A. 102:16460–16465.

Chang E, Merzenich MM. 2003. Environmental noise retards auditory cortical development. Science. 300:498–502.

Chattopadhyaya B, Di Cristo G, Higashiyama H, Knott GW, Kuhlman SJ, Welker E, Huang ZJ. 2004. Experience and activity-dependent maturation of perisomatic GABAergic innervation in primary visual cortex during a postnatal critical period. J Neurosci. 24:9598–9611.

Code R, Winer JA. 1985. Commissural neurons in layer III of cat primary auditory cortex (AI): pyramidal and non-pyramidal cell input. J Comp Neurol. 242:485–510.

Connors BW, Gutnick MJ. 1990. Intrinsic firing patterns of diverse neocortical neurons. Trends Neurosci. 13:99–104.

Cruikshank SJ, Rose HJ, Metherate R. 2002. Auditory thalamocortical transmission in vitro. J Neurophysiol. 87:361–384.

De Ribaupierre F, Goldstein MH, Jr, Yeni-Komshian G. 1972. Intracellular study of the cat's primary auditory cortex. Brain Res. 48:185–204.

de Villers-Sidani E, Chang EF, Bao S, Merzenich MM. 2007. Critical period window for spectral tuning defined in the primary auditory cortex (A1) in the rat. J Neurosci. 27:180–190.

de Villers-Sidani E, Simpson KL, Lu YF, Lin RC, Merzenich MM. 2008. Manipulating critical period closure across different sectors of the primary auditory cortex. Nat Neurosci. 11:957–965.

Doischer D, Hosp JA, Yanagawa Y, Obata K, Jonas P, Vida I, Bartos M. 2008. Postnatal differentiation of basket cells from slow to fast signaling devices. J Neurosci. 28:12956–12968.

Dorrn A, Yuan K, Barker AJ, Schreiner CE, Froemke RC. 2010. Developmental sensory experience balances cortical excitation and inhibition. Nature. 465:932–936.

Du J, Zhang L, Weiser M, Rudy B, McBain CJ. 1996. Developmental expression and functional characterization of the potassium-channel subunit Kv3.1b in parvalbumin-containing interneurons of the rat hippocampus. J Neurosci. 16:506–518.

Ehret G. 1976. Development of absolute auditory thresholds in the house mouse (Mus musculus). J Am Audiol Soc. 1:179–184.

Gingrich K, Roberts WA, Kass RS. 1995. Dependence of the GABAA receptor gating kinetics on the alpha-subunit isoform: implications for structure-function relations and synaptic transmission. J Physiol. 489:529–543.

Gonchar Y, Pang L, Malitschek B, Bettler B, Burkhalter A. 2001. Subcellular localization of GABA(B) receptor subunits in rat visual cortex. J Comp Neurol. 431:182–197.

Hensch T. 2005. Critical period plasticity in local cortical circuits. Nat Rev Neurosci. 6:877–888.

Higley M, Contreras D. 2006. Balanced excitation and inhibition determine spike timing during frequency adaptation. J Neurosci. 26:448–457.

Holmgren C, Harkany T, Svennenfors B, Zilberter Y. 2003. Pyramidal cell communication within local networks in layer 2/3 of rat neocortex. J Physiol. 551:139–152.

Insanally M, Köver H, Kim H, Bao S. 2009. Feature-dependent sensitive periods in the development of complex sound representation. J Neurosci. 29:5456–5462.

Itami C, Kimura F, Nakamura S. 2007. Brain-derived neurotrophic factor regulates the maturation of layer 4 fast-spiking cells after the second postnatal week in the developing barrel cortex. J Neurosci. 27:2241–2252.

Jeschke M, Lenz D, Budinger E, Herrmann CS, Ohl FW. 2007. Gamma oscillations in gerbil auditory cortex during a target-discrimination task reflect matches with short-term memory. Brain Res. 1220:70–80.

Kawaguchi Y, Kondo S. 2002. Parvalbumin, somatostatin and cholecystokinin as chemical markers for specific GABAergic interneuron types in the rat frontal cortex. J Neurocytol. 31:277–287.

Kobayashi M, Hamada T, Kogo M, Yanagawa Y, Obata K, Kang Y. 2008. Developmental profile of GABAA-mediated synaptic transmission in pyramidal cells of the somatosensory cortex. Eur J Neurosci. 28:849–861.

Kotak V, Fujisawa S, Lee FA, Karthikeyan O, Aoki C, Sanes DH. 2005. Hearing loss raises excitability in the auditory cortex. J Neurosci. 25:3908–3918.

Kotak VC, Takesian AE, Sanes DH. 2008. Hearing loss prevents the maturation of GABAergic transmission in the auditory cortex. Cereb Cortex. 18:2098–2108.

Kumar S, Bacci A, Kharazia V, Huguenard JR. 2002. A developmental switch of AMPA receptor subunits in neocortical pyramidal neurons. J Neurosci. 22:3005–3015.

Lakatos P, Szilagyi N, Pincze Z, Rajkai C, Ulbert I, Karmos G. 2004. Attention and arousal related modulation of spontaneous gamma-activity in the auditory cortex of the cat. Brain Res Cogn Brain Res. 19:1–9.

Lambolez B, Ropert N, Perrais D, Rossier J, Hestrin S. 1996. Correlation between kinetics and RNA splicing of alpha-amino-3-hydroxy-5-methylisoxazole-4-propionic acid receptors in neocortical neurons. Proc Natl Acad Sci U S A. 93:1797–1802.

Lefort S, Tomm C, Floyd Sarria JC, Petersen CC. 2009. The excitatory neuronal network of the C2 barrel column in mouse primary somatosensory cortex. Neuron. 61:301–316.

Linden JF, Schreiner CE. 2003. Columnar transformations in auditory cortex? A comparison to visual and somatosensory cortices. Cereb Cortex. 13:83–89.

Lu Y, Harris JA, Rubel EW. 2007. Development of spontaneous miniature EPSCs in mouse AVCN neurons during a critical period of afferent-dependent neuron survival. J Neurophysiol. 97:635–646.

MacDonald KD, Barth DS. 1995. High frequency (gamma-band) oscillating potentials in rat somatosensory and auditory cortex. Brain Res. 694:1–12.

Markram H, Wang Y, Tsodyks M. 1998. Differential signaling via the same axon of neocortical pyramidal neurons. Proc Natl Acad Sci U S A. 95:5323–5328.

Metherate R, Aramakis VB. 1999. Intrinsic electrophysiology of neurons in thalamorecipient layers of developing rat auditory cortex. Brain Res Dev Brain Res. 115:131–144.

Metherate R, Cruikshank SJ. 1999. Thalamocortical inputs trigger a propagating envelope of gamma-band activity in auditory cortex in vitro. Exp Brain Res. 126:160–174.

Ojima H, Honda CN, Jones EG. 1991. Patterns of axon collateralization of identified supragranular pyramidal neurons in the cat auditory cortex. Cereb Cortex. 1:80–94.

Ojima H, Murakami K. 2002. Intracellular characterization of suppressive responses in supragranular pyramidal neurons of cat primary auditory cortex in vivo. Cereb Cortex. 12:1079–1091.

Okaty B, Miller MN, Sugino K, Hempel CM, Nelson SB. 2009. Transcriptional and electrophysiological maturation of neocortical fast-spiking GABAergic interneurons. J Neurosci. 29:7040–7052.

Oswald A, Doiron B, Rinzel J, Reyes AD. 2009. Spatial profile and differential recruitment of GABAB modulate oscillatory activity in auditory cortex. J Neurosci. 29:10321–10334.

Oswald AM, Reyes AD. 2008. Maturation of intrinsic and synaptic properties of layer 2/3 pyramidal neurons in mouse auditory cortex. J Neurophysiol. 99:2998–3008.

Reyes A, Lujan R, Rozov A, Burnashev N, Somogyi P, Sakmann B. 1998. Target-cell-specific facilitation and depression in neocortical circuits. Nat Neurosci. 1:279–285.

Rudy B, McBain CJ. 2001. Kv3 channels: voltage-gated K+ channels designed for high-frequency repetitive firing. Trends Neurosci. 24:517–526.

Sarro EC, Kotak VC, Sanes DH, Aoki C. 2008. Hearing loss alters the subcellular distribution of presynaptic GAD and postsynaptic GABAA receptors in the auditory cortex. Cereb Cortex. 18: 2855–2867.

Schroeder CE, Lakatos P, Kajikawa Y, Partan S, Puce A. 2008. Neuronal oscillations and visual amplification of speech. Trends Cogn Sci. 12:106–113.

Seidl A, Grothe B. 2005. Development of sound localization mechanisms in the Mongolian gerbil is shaped by early acoustic experience. J Neurophysiol. 94:1028–1036.

Sun Y, Wu GK, Liu BH, Li P, Zhou M, Xiao Z, Tao HW, Zhang LI. 2010. Fine-tuning of pre-balanced excitation and inhibition during auditory cortical development. Nature. 465:927–931.

Tan A, Atencio CA, Polley DB, Merzenich MM, Schreiner CE. 2007. Unbalanced synaptic inhibition can create intensity-tuned auditory cortex neurons. Neuroscience. 146:449–462.

Tan AY, Zhang LI, Merzenich MM, Schreiner CE. 2004. Tone-evoked excitatory and inhibitory synaptic conductances of primary auditory cortex neurons. J Neurophysiol. 92:630–643.

Tansey E, Chow A, Rudy B, McBain CJ. 2002. Developmental expression of potassium-channel subunit Kv3.2 within subpopulations of mouse hippocampal inhibitory interneurons. Hippocampus. 12:137–148.

Thomson A, West DC, Wang Y, Bannister AP. 2002. Synaptic connections and small circuits involving excitatory and inhibitory neurons in layers 2-5 of adult rat and cat neocortex: triple intracellular recordings and biocytin labelling *in vitro*. Cereb Cortex. 12:936–953.

Thomson AM, Lamy C. 2007. Functional maps of neocortical local circuitry. Front Neurosci. 1:19–42.

Traub RD, Whittington MA, Stanford IM, Jefferys JG. 1996. A mechanism for generation of long-range synchronous fast oscillations in the cortex. Nature. 383:621–624.

Volkov IO, Galazjuk AV. 1991. Formation of spike response to sound tones in cat auditory cortex neurons: interaction of excitatory and inhibitory effects. Neuroscience. 43:307–321.

Wang H, Gao WJ. 2009. Cell type-specific development of NMDA receptors in the interneurons of rat prefrontal cortex. Neuropsychopharmacology. 34:2028–2040.

Wang X, Lu T, Snider RK, Liang L. 2005. Sustained firing in auditory cortex evoked by preferred stimuli. Nature. 435:341–346.

Wehr M, Zador AM. 2003. Balanced inhibition underlies tuning and sharpens timing in auditory cortex. Nature. 426:442–446.

Wehr M, Zador AM. 2005. Synaptic mechanisms of forward suppression in rat auditory cortex. Neuron. 47:437–445.

Winer J. 1984. The pyramidal neurons in layer III of cat primary auditory cortex (AI). J Comp Neurol. 229:476–496.

Winer J. 1985. Structure of layer II in cat primary auditory cortex (AI). J Comp Neurol. 238:10–37.

Wu GK, Arbuckle R, Liu BH, Tao HW, Zhang LI. 2008. Lateral sharpening of cortical frequency tuning by approximately balanced inhibition. Neuron. 58:132–143.

Wu GK, Li P, Tao HW, Zhang LI. 2006. Nonmonotonic synaptic excitation and imbalanced inhibition underlying cortical intensity tuning. Neuron. 52:705–715.

Xu J, Yu L, Cai R, Zhang J, Sun X. 2010. Early continuous white noise exposure alters auditory spatial sensitivity and expression of GAD65 and GABAA receptor subunits in rat auditory cortex. Cereb Cortex. 20:804–812.

Zhang L, Bao S, Merzenich MM. 2006. Persistent and specific influences of early acoustic environments on primary auditory cortex. Nat Neurosci. 4:1123–1130.

Zhang LI, Tan AY, Schreiner CE, Merzenich MM. 2003. Topography and synaptic shaping of direction selectivity in primary auditory cortex. Nature. 424:201–205.